Proceedings for the 13th International Winds Workshop
27 June - 1 July 2016, Monterey, California, USA

ASSIMILATION EXPERIMENTS OF HIMAWARI-8 RAPID SCAN ATMOSPHERIC MOTION VECTORS

Michiko Otsuka[1,2], Masaru Kunii[1,2], Hiromu Seko[1,2], Kazuki Shimoji[3]

[1]Meteorological Research Institute, 1-1 Nagamine, Tsukuba, Ibaraki 305-0052, Japan
[2]RIKEN Advanced Institute for Computational Science, 7-1-26 Minatojima-minami-machi, Chuo-ku, Kobe, Hyogo 650-0047, Japan
[3]Meteorological Satellite Center, 3-235 Nakakiyoto, Kiyose, Tokyo 204-0012, Japan

Abstract

Himawari-8 has been operating rapid scan observations over Japan and the neighbouring area every 2.5 minutes. Rapid Scan Atmospheric Motion Vectors (RS-AMV) are derived from the rapid scan imagery with the improved retrieval algorithm involving newly developed tracking and height assignment methods (Shimoji 2014). This study aims to investigate the impact of RS-AMVs on the prediction of mesoscale phenomena such as local heavy rainfalls.

First, the data quality and the characteristics of observation errors of RS-AMVs were examined using the statistics of differences from JMA mesoscale analyses, radiosonde and wind profiler observations and NHM (JMA non-hydrostatic model) forecasts. In order to make full use of these high resolution data and to avoid observation error correlations in space and time, the strategies for quality control, data thinning or formation of super observation should be well considered. Next, data assimilation experiments using NHM-LETKF (Kunii 2014) on a heavy rainfall event in summer of 2015 were conducted. Some cases brought promising results showing a positive impact on precipitation forecasts, though we need further investigation about how to utilize RS-AMVs in our data assimilation system more effectively.

PURPOSE

Our main interest is to improve the accuracy of short-range forecasts of heavy rainfalls and other meso-scale severe weathers by utilizing high temporal and spatial resolution RS-AMVs for assimilation. Because RS-AMVs are expected to capture smaller scale airflows than ordinary AMVs, they can be useful in mesoscale data assimilation. Some case studies showed the advantages of assimilating Himawari RS-AMVs in forecasts of havy rainfalls or typhoons (Yamashita 2010; Yamashita 2012; Otsuka et al. 2015; Kunii et al. 2016). However, the positive impacts still depend on the cases without concrete knowledge about in which space and time scale RS-AMVs could represent in the wind field. Now that Himawari-8 rapid scan operations have been bringing more data with unprecedented density and frequency, it is necessary to find the most efficient way to utilize RS-AMVs for maximum benefits in assimilation. As a necessary first step, we examined the data quality and error characteristics, and then conducted assimilation experiments on a heavy rainfall case with different settings in formation of super observations.

VERIFICATION AND OBSERVATION ERROR STATISTICS OF RS-AMV:

Before putting RS-AMVs into use for assimilation experiments, their data quality and characteristics of observation errors were examined based on the statistics of differences from JMA mesoscale analyses, radiosonde and wind profiler observations and NHM (JMA non-hydrostatic model) forecasts. Himawari-8 RS-AMVs were derived from image triplets at 5-min interval taken from 2.5-min rapid scans over the two rectangle areas around Japan (Figure 1). They were computed every 15-min for each of six bands (Table 1) using the same AMV software as used for ordinary AMVs. The horizontal resolution of the RS-AMV data set is about 0.18 degree of latitude and longtitude, and the target box size used for the computation is 5 pixels x 5 pixels . Figure 2 shows the the numbers of RS-AMVs by pressure levels for the month of August 2015. Thanks to the improvement in AMV software and the increased number of bands, Himawari-8 enabled to obtain many more low and middle level winds than MTSATs as well as high level winds.

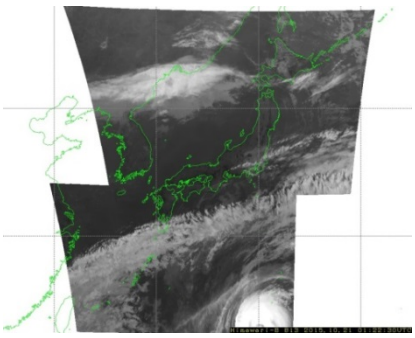

Figure 1: **2.5-min rapid scan area around Japan by Himawari-8.**

	Wave length [μm]
B03	0.64
B07	3.90
B08	6.20
B09	6.90
B10	7.30
B13	10.4

Table 1: **Six bands used for AMV retrieval.**

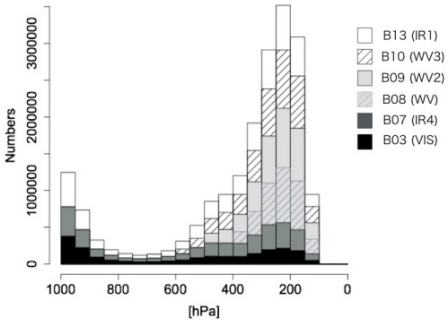

Figure 2: **Distributions of observations according to pressure level.**

Verification of RS-AMV:

Firstly, RS-AMVs were compared with JMA mesoscale analysis. Table 2 shows the differences (RS-AMV minus JMA meso analysis) averaged over the whole period of August 2015. The root mean square vector differences (RMSVDs) in VIS or IR (B03, B07 and B13) channels were around 5.2 - 5.7 m s^{-1}, while those in WV channels (B08, B09 and B10) were 6.5 - 6.9 m s^{-1}. The root mean square differences (RMSDs) for u- and v- component and wind speed were also slightly larger in WV than in VIS and IR channels, and slight positive biases were noticeable in the mean differences (MDs) for u-component and wind speed in WV channels, especially in B08. The shapes of histograms of differences for u- and v – component (Figure 3) were close to Gaussian distribution and seemed good enough to be assimilated. The comparisons with sonde (Table 3) and wind profiler (Table 4) observations brought similar results with a little larger RMSVDs, RMSDs and MDs for WV RS-AMVs than those of VIS and IR. Figure 4 maps out the GPS radiosonde and wind profiler stations in the JMA's observation network used for the comparisons.

In Table 5, 6 and 7, the statistics were separately taken for each group of three different height categories, low (below 700 hPa pressure level), middle (700 - 400 hPa) and high (above 400 hPa) for VIS and IR channels (B03, B07 and B13). Low and mid-level RS-AMVs which number of data has dramatically increased thanks to the new retrieval software seem to be of good quality. In particular, low-level RS-AMVs were in good agreement with wind profiler observations (Table 7) including winds over land. Low-level AMVs over land have not been used in operational NWP of JMA. However, we used them in this study because they could possibly capture characteristic wind features near surface that is useful for mesoscale prediction. Himawari-8 enabled to produce mid- and high-level VIS (B03) AMVs that were not available by MTSATs. They showed slight negative biases at mid-levels in comparison with JMA meso analysis and wind profiler (Table 5 and 7), while their RMSDs against sonde were relatively large at high levels (Table 6). It is not yet known why substantial positive biases against wind profiler observations were seen at high levels in all the three channels.

Most RS-AMVs during the period were flagged with high QI (Holmlund 1998), and not a single RS-AMV had a QI below 0.70 (Figure 5). It may be necessary to set the QI threshold higher or introduce an additional QC more suitable for high resolution AMVs in the future. RMSVDs against JMA mesoscale analysis with QI below 0.90 were significantly large in WV channels (Table 8), indicating a QI threshold value such as 0.90 or higher should be appropriate for WV RS-AMVs when they are used in assimilation.

	RMSVD (m s^{-1})	RMSD (m s^{-1})		MD (m s^{-1})		RMSD (m s^{-1}) speed	MD (m s^{-1}) speed
		u	v	u	v		
B03	5.19	3.74	3.60	-0.11	0.08	3.67	-0.14
B07	5.40	3.92	3.72	-0.21	0.24	3.74	-0.24
B08	6.93	4.96	4.83	0.70	0.32	4.96	1.05
B09	6.70	4.80	4.67	0.50	0.20	4.74	0.73
B10	6.50	4.64	4.55	0.34	0.18	4.59	0.48
B13	5.72	4.12	3.97	0.09	0.17	3.95	0.04

Table 2: **RMSVD, RMSD and MD values of RS-AMVs at each band relative to JMA meso analysis.**

	RMSVD (m s^{-1})	RMSD (m s^{-1})		MD (m s^{-1})	
		u	v	u	v
B03	7.17	5.33	6.37	-0.18	0.17
B07	6.97	5.18	4.66	-0.22	0.14
B08	8.38	6.19	5.66	0.73	0.13
B09	8.13	6.00	5.48	0.56	0.05
B10	7.89	5.83	5.31	0.42	0.07
B13	7.22	5.35	4.86	0.13	0.04

Table 3: **RMSVD, RMSD and MD values of RS-AMVs at each band relative to sonde observations. Distance < 150 km, 25 hPa. Time difference < 1.5 hrs.**

	RMSVD ($m\ s^{-1}$)	RMSD ($m\ s^{-1}$)		MD ($m\ s^{-1}$)		RMSD ($m\ s^{-1}$) speed	MD ($m\ s^{-1}$) speed
		u	v	u	v		
B03	5.62	4.10	3.84	0.31	-0.37	4.12	-0.03
B07	5.61	4.09	3.85	0.46	-0.32	4.08	0.07
B08	7.58	5.58	5.12	2.55	-0.38	5.49	2.34
B09	7.26	5.25	5.01	1.89	-0.54	5.16	1.61
B10	6.71	4.83	4.65	1.41	-0.49	4.77	1.08
B13	5.92	4.29	4.08	0.72	-0.35	4.23	0.34

Table 4: **RMSVD, RMSD and MD values of RS-AMVs at each band relative to wind profiler observations. Distance < 50 km, 10hPa. Time difference < 5 min.**

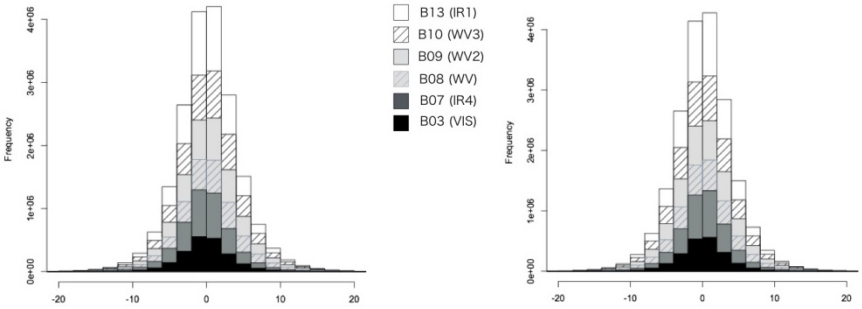

Figure 3: **Distributions of differences of u and v components ($m\ s^{-1}$) between RS-AMVs and JMA meso analysis winds. U components (left) and v components (right).**

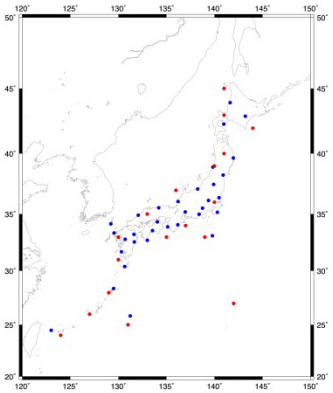

Figure 4: **Sonde (red circles) and wind profiler (blue circles) stations of JMA.**

		RMSD ($m\ s^{-1}$)		MD ($m\ s^{-1}$)		RMSD ($m\ s^{-1}$) speed	MD ($m\ s^{-1}$) speed	Number of Data
		u	v	u	v			
Low	**B03**	2.81	2.69	-0.17	0.17	2.78	0.07	824260
	B07	2.82	2.61	-0.08	0.21	2.63	-0.13	897445
	B13	3.17	2.85	0.27	0.14	2.82	0.00	1040863
Mid	**B03**	3.81	3.66	-0.36	-0.19	3.71	-0.49	430196
	B07	4.14	3.83	-0.35	0.05	3.88	-0.36	681348
	B13	4.30	4.07	-0.17	-0.08	4.08	-0.20	897807
High	**B03**	4.40	4.24	0.06	0.13	4.32	-0.17	888181
	B07	4.36	4.20	-0.22	0.35	4.22	-0.25	1489376
	B13	4.40	4.32	0.11	0.27	4.30	0.15	2462821

Table 5: **RMSVD, RMSD and MD values of VIS and IR RS-AMVs relative to JMA meso analysis.**

		RMSD ($m\ s^{-1}$)		MD ($m\ s^{-1}$)		RMSD ($m\ s^{-1}$) speed	MD ($m\ s^{-1}$) speed	Number of Data
		u	v	u	v			
Low	**B03**	3.74	3.28	0.23	-0.06	3.59	-0.04	37473
	B07	3.79	3.40	0.42	0.09	3.60	-0.18	42120
	B13	4.00	3.67	0.62	0.15	3.75	0.09	51575
Mid	**B03**	4.12	3.93	-0.40	-0.59	4.17	-0.79	75665
	B07	4.05	3.93	-0.15	-0.57	4.12	-0.54	123700
	B13	4.23	4.15	-0.07	-0.64	4.22	-0.45	154125
High	**B03**	4.10	3.84	1.01	-0.32	4.28	0.67	82524
	B07	3.91	4.22	1.08	-0.22	4.19	0.77	124757
	B13	4.43	4.14	1.48	-0.24	4.38	1.15	166021

Table 7: **RMSVD, RMSD and MD values of VIS and IR RS-AMVs relative to wind profiler observations.**

	RMSD ($m\ s^{-1}$)		MD ($m\ s^{-1}$)	
	u	V	u	v
Low **B03**	3.90	3.69	0.20	0.00
B07	3.89	3.59	0.29	-0.14
B13	4.18	3.73	0.57	-0.26
Mid **B03**	4.48	4.19	-0.63	-0.56
B07	4.53	4.25	-0.47	-0.49
B13	4.87	4.53	-0.27	-0.56
High **B03**	6.37	5.59	-0.17	0.65
B07	5.72	5.08	-0.26	0.48
B13	5.69	5.15	0.16	0.30

Table 6: **RMSVD, RMSD and MD values of VIS and IR RS-AMVs relative to sonde**

	QI		
	0.8-0.9	**0.9-0.1**	**1**
B03	5.47	3.98	3.59
B07	8.65	4.07	3.65
B08	14.39	7.28	4.64
B09	12.12	6.91	4.62
B10	10.62	6.62	4.56
B13	6.18	4.45	4.03

	QI		
	0.8-0.9	**0.9-0.1**	**1**
B03	5.16	4.43	3.91
B07	5.30	4.62	5.03
B08	10.50	7.73	6.76
B09	9.31	7.31	6.28
B10	8.61	6.80	6.12
B13	5.66	4.79	4.51

Table 8: **Difference from JMA meso analysis by QI thresholds (RMSVD [m/s]). QI values with forecast (top) and without forecast (bottom).**

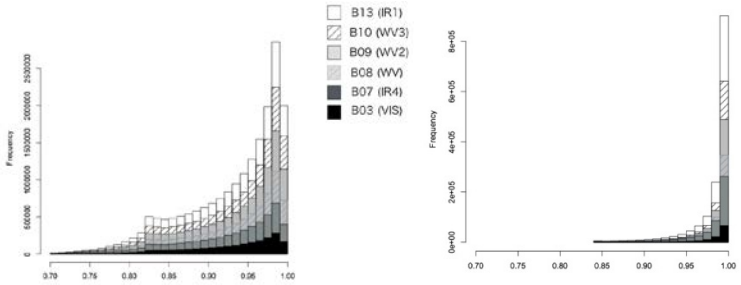

Figure 5: **Distributions of observations according to QI values. QI with forecast (left) and QI without forecast (right).**

Correlation of observation errors:

We estimated horizontal and inter-band correlations of observation errors based on the statistics of covariances of first-guess departures (RS-AMV minus NHM forecast wind). In Figure 6, correlations between pairs of observations in B03 and B13 within 3-h time window were calculated and binned by spatial distance between the two observations and the contents of each bin were averaged over the period of 1st – 15th August 2015. The average correlation for low-level RS-AMVs is below 0.2 around 200 km, while the correlations of mid- and high-level RS-AMVs are still high at the same distance. The correlations for other bands than B03 and B13 showed the same tendencies (not shown here). It is necessary to consider these possible spatial correlations of observation errors when assimilating such high-density data as RS-AMVs.

As for the inter-band correlations, correlations between pairs of observations from different bands within 25-k m horizontal and 25-hPa vertical distance and the same 3-h time window were computed and averaged over the period by different combinations of two bands (Table 9). The averages of correlations were calculated separately for the three height categories. The correlations were higher in pairs of RS-AMVs at higher levels without depending on certain band combinations.

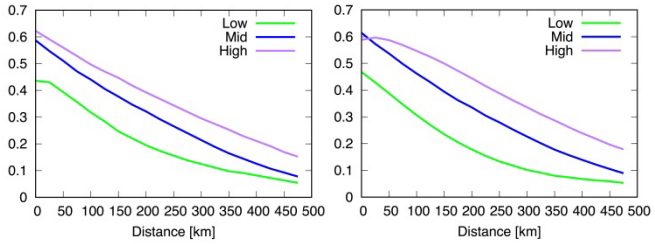

Figure 6: **Estimated spatial observation error correlations as a function of the distance (km) between pairs of RS-AMVs. U-component of B03 (left) and B13 (right).**

		B03	B07	B08	B09	B10	B13
B03	**Low**		0.44	-	-	-	0.45
	Mid		0.56	-	0.55	0.56	0.57
	High		0.59	0.61	0.62	0.62	0.62
B07	**Low**			-	-	-	0.46
	Mid			-	0.57	0.58	0.59
	High			0.63	0.63	0.63	0.63
B08	**High**				0.63	0.63	0.63
B09	**Mid**					0.60	0.57
	High					0.63	0.63
B10	**Mid**						0.59
	High						0.63

Table 9: **Estimated inter band observation error correlations.**

ASSIMILATION EXPERIMENTS:

Method:

We conducted assimilation experiments of RS-AMVs with NHM-LETKF (the local ensemble transform Kalman filter implemented with NHM). The assimilation domain was almost the same size as used for JMA operational meso-analysis (Figure 7) with a horizontal resolution of 15 km and 50 vertical levels. The ensemble size was 50, and the localization scale was 200 km in horizontal and 0.2 hPa in vertical. RS-AMVs were assimilated in 1-h time slots within each 3-h assimilation window as well as other observational data used for JMA meso-analysis.

The assimilation experiments were performed for a summer heavy rainfall event on 16 August 2015 caused by a front and low pressure system. One-hour rainfall totals of 60 – 70 mm or more were observed in western and eastern Japan. Severe weathers such as small-scale tornadoes and wind gusts were also reported in the Kanto Region in eastern part of the country. The first NHM-LETKF cycle started six days before at 00 UTC on 10 August taking sufficient time of spin-up. In the test case (TEST), RS-AMVs were

assimilated every hour for 6 cycles from 00 UTC to 18 UTC on 16 August. While in the control case (CNTL), only observational data used for operational JMA meso-analysis were assimilated. Next, 12-h extended forecasts for a smaller domain (Figure 8) with a resolution of 5 km and 60 vertical levels were conducted using the analysis of the ensemble mean at 18 UTC as initial conditions. Then we compared the forecasts of TEST and CNTL to see the impact of RS-AMVs.

Formation of super observation:

RS-AMVs were assimilated in the form of super observations. All the RS-AMVs in area of 50 km x 50 km at lower levels and 100 km x 100 km at mid or high levels were averaged because horizontal error correlations of mid- and high RS-AMVs were higher than those at low levels. Also based on the statistics, the three bands, B03, B10 and B13 were selected among the six bands. The exclusion of the other two WV channels, B08 and B09, was intended to avoid excessive positive biases. B07 was not used in order to reduce redundancy because its coverage was similar to B03 and B13. RS-AMVs in the selected three bands were formed into one super observation every hour on the hour. The example of superobbed RS-AMVs is shown in Figure 9. Observation errors of RS-AMVs were set to the same values as used for ordinary AMVs in JMA meso analysis.

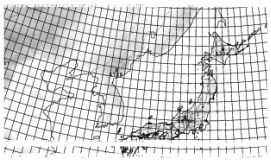

Figure 7: **The assimilation domain of NHM-LETKF. Metres above sea level is indicated by shading.**

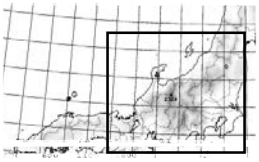

Figure 8: **The forecast domain of NHM. The rectangle indicates the target area for precipitation forecast validation.**

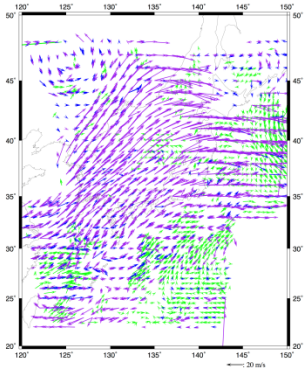

Figure 9: **Example of super-observation of RS-AMVs. Green, blue and purple vectors indicate winds at low, mid and high levels, respectively.**

RESULTS OF ASSIMILATION EXPERIMENTS

Increments (analysis minus first guess) of u- and v- component at initial time were reasonable agreement with RS-AMV observations assimilated during the cycle, for example, low winds around over the southern sea and high winds in the northern part (not shown). The differences of analyses between TEST and CNTL also reflected the effect from the added observations.

Forecast winds by TEST and CNTL were evaluated against wind profiler observations. RMSVDs at each forecast time up to 12 hours and RMSEs averaged over the forecast period for TEST and CNTL are shown in Figure 10. The RMSVD was better in TEST at early hours of forecast but worse after 5-hour, while RMSEs seemed better at lower levels.

We compared the 3-hour amount rainfall of TEST and CNTL at each forecast time. The forecast scores (threat score and bias score) were calculated over the intense rainfall area in part of the forecast domain (the rectangle area in Figure 8) based on validation against observations by radar and rainguage rainfall analysis. Three different experiments other than TEST were conducted with each using a different resolution of smoothing or different bands in the formation of super observations (Table 10). The two additional experiments were also conducted, one is LOW where only low-level winds were assimilated, while in the other (MidUp), only mid and high level winds were employed. Results from each experiment are compared with each other to see the importance of data selection and smoothing of the data before assimilation.

Threat and bias scores of TEST, CNTL, and the other three tests where superobbing resolution or band selection was different from TEST were averaged over the whole forecast period (Figure 12). TEST overall tended to underestimate precipitation showing slightly better scores for light rain but worse in case of heavy rain than CNTL. LMU50 and AllBndLMU50 where superobbing resolution was 50 km from bottom to top seemed better than TEST, while LMU100 and AllBndLMU100 with a resolution of 100 km were worse than TEST. AllBnd where all the six bands were used was slightly worse than TEST in threat score though better at some thresholds in bias score. Threat scores of LOW were overall better than those of TEST and MidUp

especially in the range of high thresholds (Figure 12). In MidUp, a tendency to underestimate was more significant than in TEST. We still need further investigation to find the best options for the scale of spatial smoothing, the band selection and other settings for superobbing as well as QC, observation errors in order to get the best out of high resolution RS-AMVs.

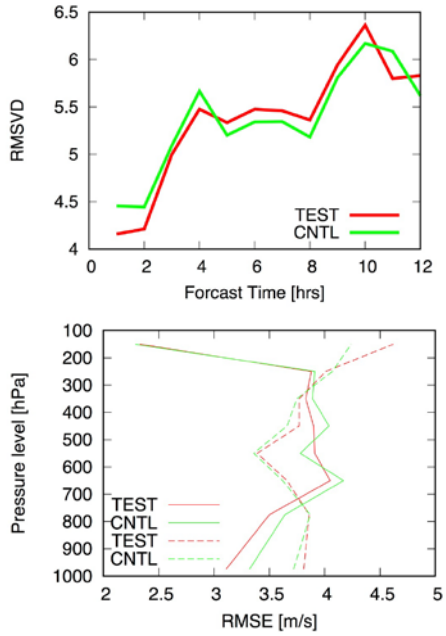

Figure 10: **Forecast winds validated against wind profiler winds. RMSVD [m/s] at each forecast time (top). RMSE profiles for u- (solid line) and v- (dashed line) component (bottom).**

Name of experiments	Level of AMVs assimilated	Band of AMVs assimilated	Resolution of smoothing for super-obbing
TEST	All	B03, B10, B13	50 km (Low) 100 km (Mid, High)
AllBnd	All	All	50 km (Low) 100 km (Mid, High)
LMU50	All	B03, B10, B13	50 km
AllBndLMU50	All	All	50 km
LOW	Low	B03, B10, B13	50 km
MidUp	Mid, High	B03, B10, B13	100 km

Table 10: **Description of assimilation experiments with RS-AMVs.**

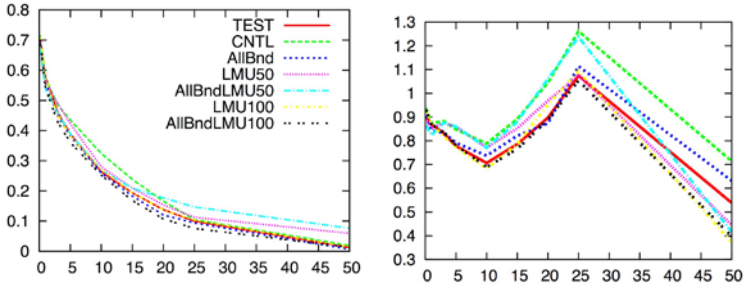

Figure 11**: Precipitation forecast scores for the experiments with different setting in super-obbing. Threat score (left) and bias score (right) averaged over the whole forecast period at each threshold of 3-h amount of rainfall [mm].**

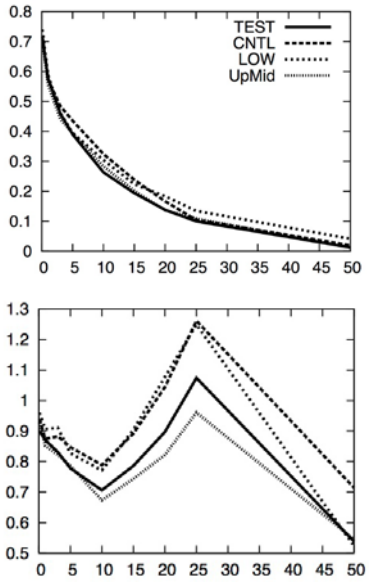

Figure 12**: Precipitation forecast scores for the experiments using winds at different levels. Threat score (top) and bias score (bottom).**

CONCLUSION

The data quality and the characteristics of observation errors of RS-AMVs were examined using the statistics of differences from JMA mesoscale analyses, radiosonde and wind profiler observations and NHM forecasts. We need to consider the different data characteristics at different height in different channels that were revealed in the results when utilizing RS-AMVs into assimilation.

Data assimilation experiments using NHM-LETKF on a heavy rainfall event were conducted to see the impact of RS-AMV on analyses and forecasts of wind and rainfall. The impact of RS-AMV was slightly positive in wind forecasts, while in rainfall forecasts, slightly positive in case of light rain but negative in heavy rain. We still need further investigation in the methods of data selection in order to take advantage of these high resolution RS-AMVs.

Observation error correlation in time was not taken into account in this preliminary experiment, as only hourly data were assimilated. To realize assimilation with higher resolution and frequency, it should be considered in the future study.

ACKNOWLEDGEMENTS

This research was supported by JST, CREST, as part of “Innovating “Big Data Assimilation technology for revolutionizing very-short-range severe weather prediction” (PI: Dr. Takemasa Miyoshi).

REFERENCES

Holmlund, K., 1998: The utilization of statistical properties of satellite-derived atmospheric motion vectors to derive quality indicators. *Wea*. *Forecasting*, 13, 1093-1104.

Kunii M., 2014: Mesoscale data assimilation for a local severe rainfall event with the NHM-LETKF system. *Wea. Forecasting*, 29, 1093-1105.

Kunii M., M. Otsuka, K. Shimoji, and H. Seko 2016: Ensemble data assimilation and forecast experiments for the September 2015 heavy rainfall event in Kanto and Tohoku Regions with atmospheric motion vectors from Himawari-8. *SOLA*,12, 209−214.

Otsuka, M., M. Kunii, H. Seko, K. Shimoji, M. Hayashi, and K. Yamashita, 2015: Assimilation experiments of MTSAT rapid scan atmospheric motion vectors on a heavy rainfall event. *J. Meteor. Soc. Japan*, 93, 459−475.

Shimoji, K., 2014: Motion tracking and cloud height assignment methods for Himawari-8 AMV, *Proceedings of 12th International Winds Workshop* (Available online at http://www.eumetsat.int/website/home/News/ConferencesandEvents/PreviousEvents/DAT_2441511.html accessed on 20 September 2016).

Yamashita, K., 2010: Observing system experiments of MTSAT-2 rapid scan atmospheric motion vector for T-PARC 2008 using the JMA operational NWP system. *Proceedings of 10th International Winds Workshop* (Available online at http://www.eumetsat.int/website/home/News/ConferencesandEvents/PreviousEvents/DAT_2042632.html. accessed on 20 September 2016)

Yamashita, K., 2012: An observing system experiment of MTSAT-2 rapid scan AMV using JMA meso-scale operational NWP system. *Proceedings of 11th International Winds Workshop* (Available online at http://www.eumetsat.int/website/home/News/ConferencesandEvents/PreviousEvents/DAT_2039311.html. accessed on 20 September 2016)